JACS
JOURNAL OF THE AMERICAN CHEMICAL SOCIETY
pubs.acs.org/JACS
Article

Ion Pairing Enables Targeted Prodrug Activation via Red Light Photocatalysis: A Proof-of-Concept Study with Anticancer Gold Complexes

Zhiying Xie,[¶] Bei Cao,[¶] Jing Zhao,[¶] Moyi Liu,[¶] Yuhan Lao, Hejiang Luo, Zhi Zhong, Xiaolin Xiong, Wei Wei,* and Taotao Zou*

Cite This: J. Am. Chem. Soc. 2024, 146, 8547−8556
Read Online

ACCESS | Metrics & More | Article Recommendations | Supporting Information

ABSTRACT: Photocatalysis has found increasing applications in biological systems, for example, in localized prodrug activation; however, high-energy light is usually required without giving sufficient efficiency and target selectivity. In this work, we report that ion pairing between photocatalysts and prodrugs can significantly improve the photoactivation efficiency and enable tumor-targeted activation by red light. This is exemplified by a gold-based prodrug (**1d**) functionalized with a morpholine moiety. Such a modification causes **1d** to hydrolyze in aqueous solution, forming a cationic species that tightly interacts with anionic photosensitizers including Eosin Y (**EY**) and Rose Bengal (**RB**), along with a significant bathochromic shift of absorption tailing to the far-red region. As a result, a high photoactivation efficiency of **1d** by **EY** or **RB** under low-energy light was found, leading to an effective release of active gold species in living cells, as monitored by a gold-specific biosensor (GolS-mCherry). Importantly, the morpholine moiety, with pK_a ~6.9, in **1d** brings in a highly pH-sensitive and preferential ionic interaction under a slightly acidic condition over the normal physiological pH, enabling tumor-targeted prodrug activation by red light irradiation in vitro and in vivo. Since a similar absorption change was found in other morpholine/amine-containing clinic drugs, photocages, and precursors of reactive labeling intermediates, it is believed that the ion-pairing strategy could be extended for targeted activation of different prodrugs and for mapping of an acidic microenvironment by low-energy light.

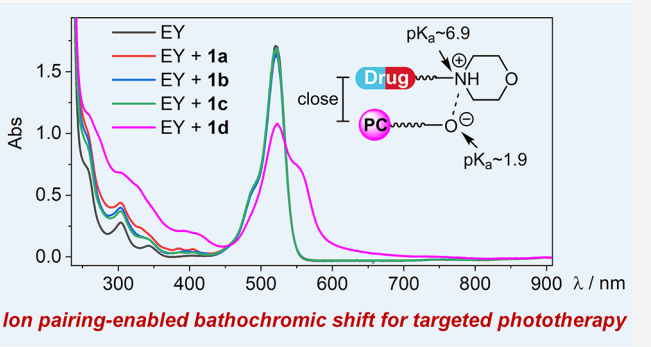

Ion pairing-enabled bathochromic shift for targeted phototherapy

INTRODUCTION

Known for its capability to generate highly reactive species under localized regions, photocatalysis has been demonstrated as a useful tool in medicinal chemistry and chemical biology.[1−4] In general, the localized activation by light within disease tissues can benefit a lot by minimizing the toxic side effects,[5−10] as exemplified by photodynamic therapy (PDT) that has been clinically exploited as a potent strategy for cancer killing.[11−15] Nevertheless, the hypoxic tumor microenvironment makes it difficult to implement PDT widely in vivo. To this end, photoactivatable prodrugs, particularly photoactivated chemotherapy, based on photoinduced uncaging of active drug molecules or opening of active metal coordination sites have been developed.[16−19] In the literature, endeavors on both inorganic and organic photoactivatable compounds have shown great potential for cancer treatment by taking advantage of the intrinsic photochemical properties of prodrugs [Scheme 1A(i)] or by additionally introducing chromophore functional groups [Scheme 1A(ii)].[20−25] Based on these strategies, a series of successful examples including those red light-activated prodrugs with multifunctions have been achieved.[8,26−29] Alternatively, the prodrugs can be activated by photocatalysis, which uses external photosensitizers and does not require the light-absorbing feature of prodrugs [Scheme 1B(i)].[30−33] Nevertheless, the efficiency of bimolecular photocatalytic activation processes is largely interfered with by the complex physiological environment; also, the photocatalysts do not naturally offer disease tissue specificity. Therefore, it is of great value to explore an efficient photocatalytic strategy for targeted prodrug activation.

In the literature, it is known that electrostatic interaction is critical in determining the conformation, dynamics, and function of biomolecules.[34] In the meantime, in photoredox catalysis, the counterions could significantly influence the

Received: January 10, 2024
Revised: March 1, 2024
Accepted: March 1, 2024
Published: March 18, 2024

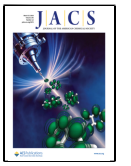

Scheme 1. Concept of Ion-Pairing Photocatalysis for Prodrug Activation[a]

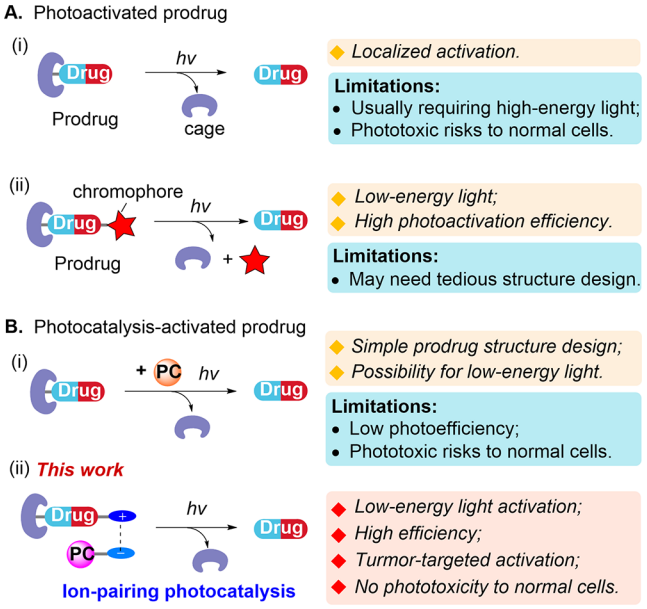

[a](A) Advantages and limitations of classical photoactivatable prodrugs without (i) or with (ii) an additional photo-absorbing chromophore. (B) Photocatalysis for prodrug activation (i) and how the ion-pair strategy in this work addresses the challenges (ii).

charge distribution of cationic photocatalysts giving divergent photoreactivities.[35−37] Therefore, we conceived that the ion-pair strategy consisting of charged prodrugs and a long-wavelength-absorbing photosensitizer may boost the photo-therapeutic efficacy [Scheme 1B(ii)]. In view that reactive gold complexes are strong thiol-enzyme inhibitors[38−42] with promising anticancer potential to overcome cisplatin resistance[43−52] and its bioactivities can be effectively tuned by ligand modification for prodrug development,[53−63] we started to employ the gold-based metallodrug as a proof-of-concept study to demonstrate the power of ion pairing in photocatalytic prodrug activation.

Herein, we report that ion-pair photocatalysis can trigger efficient and targeted prodrug activation by low-energy light. This was demonstrated via a gold(III)-hydride prodrug[64] (**1d**) functionalized with a pH-sensitive morpholine moiety in combination with an anionic photocatalyst Eosin Y (**EY**) or Rose Bengal (**RB**). The two long-wavelength-absorbing xanthene dyes can efficiently activate the thiol reactivity of **1d** with full conversion time dropped to tens of seconds. In aqueous solution, ion pairing between **EY**/**RB** and **1d** is featured by a bathochromic shift of absorption to the deep-red region. This leads to red light-activated release of active gold species in living cells and potent inhibition of thioredoxin reductase (TrxR). Of note, this red-absorbing ion pair is more tightly formed under a weak acidic environment, rendering a selective prodrug photoactivation and targeted anticancer activities in vitro and in vivo. To the best of our knowledge, it is the first time that the ion-pairing strategy was used to enable efficient and targeted photocatalytic prodrug activation by red light. Since the weak acid-favored ion-pairing and bathochromic-shift phenomena were also observed in morpholine (amine)-containing clinic drugs, photocages, and precursors of reactive labeling intermediates, this ion-pairing strategy is believed to be of potential to expand the repertoire of chemical tools for medicinal and biological applications.

RESULTS AND DISCUSSION

Synthesis, Characterization, and Stability of the Gold(III)-Hydride Complexes. The cyclometalated gold(III)-hydride complex **1d** containing a morpholine moiety (Figure 1) was prepared with a slightly modified procedure,[64]

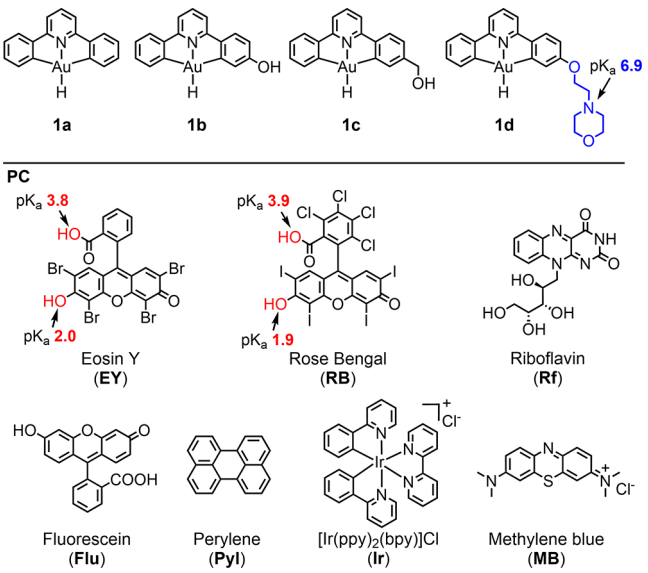

Figure 1. Chemical structures. The structures of gold(III)-hydride complexes **1a**−**1d** and different photocatalysts used in this work were shown. The pK_a values of compounds **1a**, **EY**, and **RB** are shown.

where the [Au^{III}(C∧N∧C)Cl] was synthesized via a mercury-free photochemical reaction starting from diazonium salts and dimethyl sulfide-gold(I) chloride (Cl−Au−SMe$_2$) using blue LED light.[65] The final product was fully characterized by ^{1}H NMR, ^{13}C NMR, mass spectrometry, HPLC, and elemental analysis (Figure S1). Complexes **1b** and **1c** containing hydroxyl groups were prepared for comparative study (please see the details of synthesis and characterization in Supporting Information). All of the complexes are soluble in common organic solvents such as THF, CH_2Cl_2, $CHCl_3$, DMF, and DMSO. Unless otherwise specified, the gold(III) complexes were dissolved in DMSO to prepare a 10 mM stock, which was then diluted in aqueous solution for subsequent experiments. Complexes **1b**−**1d** displayed obviously improved solubility than **1a** after dilution in aqueous solution (i.e., without forming precipitates at 200 μM).

The stability of functionalized gold(III) complexes **1d** was studied. As shown in Figure S2a, after incubating **1d** with a 5-fold excess of *N*-acetyl cysteine (NAC) in DMSO-d_6 at room temperature for 24 h, there was no noticeable changes in the ^{1}H NMR spectra. After treating human colorectal cancer cell line HCT116 with 100 μM of **1d** for 12 h in the dark, HPLC analysis of the supernatant of cell lysates after acetone precipitation showed that there was a high content of intact **1d** with no new peaks in the LC chromatograms (Figure S2b). Thus, the functionalization of **1d** with a morpholine moiety did not alter its high stability against biorelevant thiols.

Activating the Gold(III)-Hydride Complex by Photocatalysis. Then we tested if external photosensitizers can activate the gold(III)-hydride complex. Complex **1d** (100 μM)

https://doi.org/10.1021/jacs.4c00408
J. Am. Chem. Soc. 2024, 146, 8547−8556

was coincubated with 10% molar concentration of different photocatalysts (Figure 2) and 10 mM of NAC in DMSO and

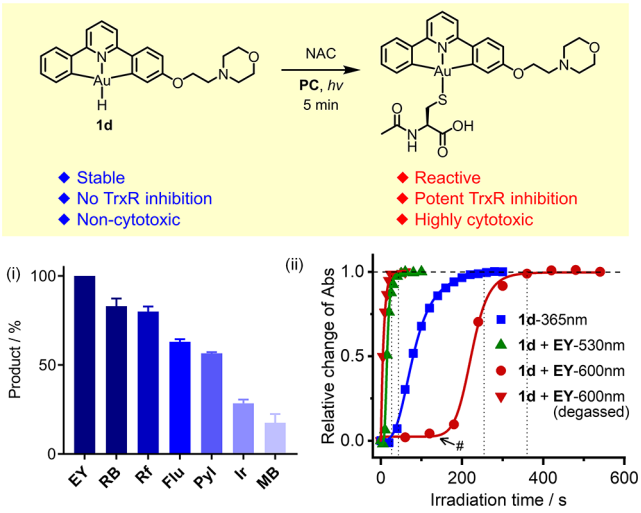

Figure 2. Photocatalytic activation of **1d** by **EY** and the proposed reaction mechanism. (a) Upper panel: photocatalytic transformation of **1d** into the Au(III)−S adduct in the presence of a 100-fold excess of NAC; lower panel: (i) reaction yields in the presence of different photocatalysts after photoirradiation for 5 min based on HPLC analysis; (ii) change of OD_{347nm} of **1d** under 365 nm UV irradiation or **1d** with **EY** under 530 or 600 nm light irradiation (#the lag time is due to oxygen consumption[33]).

irradiated with light of different wavelengths based on their low energy absorption maxima. After 5 min of irradiation, HPLC showed that these photocatalysts can produce the Au(III)−S(NAC) adduct with different efficiencies, in which the anionic **EY** and **RB** under 530 nm irradiation outperformed other photosensitizers giving product yields of 100 and 83%, respectively (Figure S3). Since the gold(III)-hydride complex itself is photoreactive under UV light,[64] we compared the photoreactivity of **1d** under UV or with **EY** under long-wavelength light irradiation. The UV−vis absorption spectra show, in Figures 2(ii), and S4, that as the reaction proceeds under UV irradiation, the absorbance of **1d** at 365−400 nm increased and reached a plateau by 270 s; of note, in the mixture of **1d** and **EY** and under 530 nm irradiation, the absorbance of **1d** quickly changed and leveled off by ∼50 s, and even under 600 nm irradiation, the reaction began to level out at 360 s [Figure 2(ii)], indicative of a very efficient photocatalytic activation by **EY**. Along with the fast change of absorbance of **1d** in the UV region, the absorbance of **EY** (at OD_{530nm}) quickly decreased over time (Figure S4), implying that the activation of **1d** is associated with reduction of **EY**.[66]

Then we tried to understand the mechanism of photoactivation. The emission quenching experiment showed that NAC, rather than **1d**, efficiently quenched the emission intensity of **EY** (Figure S5a), which is consistent with the photoredox mechanism.[67,68] Since a radical is likely formed during photoredox catalysis,[35] the reaction mixture of **1a** and **EY** was added with 2 equiv of free radical 2,2,6,6-tetramethylpiperidin-1-yloxy (TEMPO), which largely inhibited the photoreaction with <5% conversion of **1d** based on HPLC analysis (Figure S5b), suggestive of involvement of radical species.[69] Then, we tried to capture the radical intermediates. When the radical trap, 1,1-diphenylethylene, was added in the reaction mixture, the addition products with NAC (thiyl radical) and **1d** [gold(II) radical] were found by HRMS (Figure S6). Also, with an allyl-TEMPO radical trap,[70] both the gold(II) radical to allyl addition product (from HRMS) and strong EPR signals of TEMPO were observed (Figure S7), suggesting the involvement of the gold(II) radical and thiyl radical in the photoactivation. In the DFT calculation, the single-electron-reduced product $EY^{\bullet-}$ has a typical carbon-centered radical character (Figure S5c), which may abstract a hydrogen atom from the gold(III)-hydride complex.[67,68,70,71] Based on these observations, the following mechanism is proposed (Figure S8): after light irradiation, the excited **EY** can oxidize NAC via single-electron transfer (SET), generating a thiyl radical and an $EY^{\bullet-}$ radical. The latter (or possibly the thiyl radical) can abstract a hydrogen atom from **1d** forming a gold(II) radical that can recombine with the thiyl radical. This leads to formation of the Au(III)−S(NAC) adduct and a reduced **EY** that could be reoxidized into **EY**.

Ion Pairing and Bathochromic-Shifted Absorption in Aqueous Solution. Since **EY** is highly acidic with pK_{a1} = 2.0 and pK_{a2} = 3.8,[72] whereas the morpholine in **1d** is a weak base (pK_a = 6.9),[73] there should be an acid−base reaction in the mixture. When **1d** and **EY** were mixed together in DMSO-d_6, ^{1}H NMR analysis (Figure 3a) showed significant chemical shifts for the ^{1}H signals around the morpholine moiety of **1d**

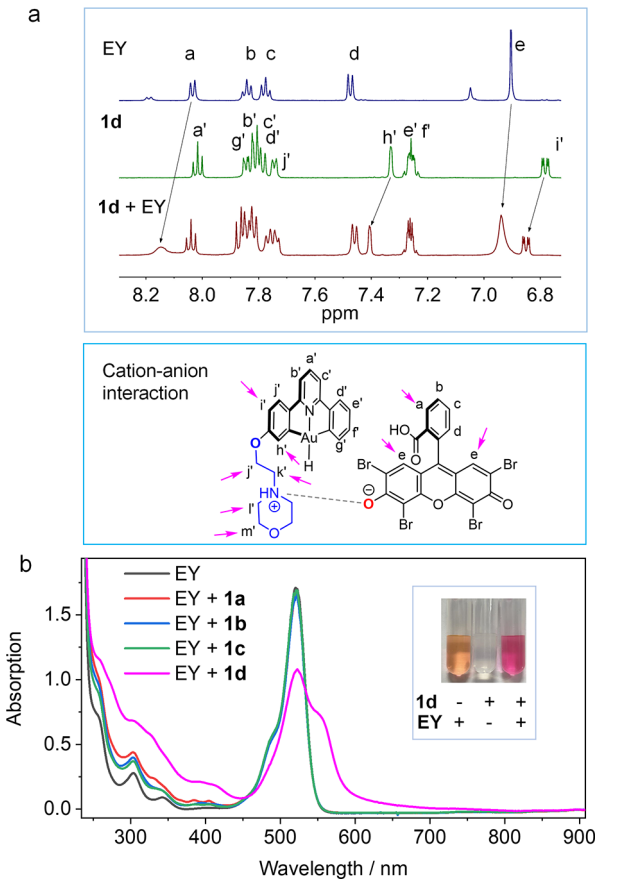

Figure 3. Formation of ion pairs. (a) ^{1}H NMR spectra for **EY**, **1d**, and the mixture in DMSO-d_6. The inset shows the proposed interacting model. (b) UV−vis absorption spectra of **EY** with or without equal molar concentration of **1a**, **1b**, **1c**, or **1d** in DMSO/H_2O (1/9, v/v) solution. The inset gives the picture of **1d**, **EY**, or the "**1d** + **EY**" mixture.

https://doi.org/10.1021/jacs.4c00408
J. Am. Chem. Soc. 2024, 146, 8547−8556

and near the hydroxyl and carboxylate groups of **EY**, which is typical of an acid−base reaction. For comparison, in the mixture of **EY** and **1a** without the morpholine group, there was no change of ^{1}H signals compared to individual compounds (Figure S9).

Interestingly, when the "**1d** + **EY**" mixture was diluted in aqueous solution (H_2O/DMSO = 9/1, v/v), a significant color change of **EY** from pink to rose red was observed (Figure 3b inset). In the UV−vis absorption spectra, there is an obvious bathochromic shift of the "**1d** + **EY**" mixture with a shoulder peak at ∼560 nm in association with a long tail approaching the near-infrared region (750−800 nm, Figure 3b), whereas **EY** alone, peaked at 530 nm, did not show absorption beyond 560 nm. The absorption spectra for the mixture of **EY** with **1a**, **1b**, or **1c** were similarly recorded; however, no change of absorption in the visible region was found (Figure 3b). Instead, morpholine itself, at a high concentration, can induce the red-shifted absorption (Figure S10a), indicating that it is the morpholine moiety that contributed to the color change. Complex **1d** similarly triggered a significant bathochromic shift with **RB** (Figure S10b,c). A possible explanation for the bathochromic shift is the high polarizability of the xanthene dye that results in a distinct change of frontier orbitals upon ion pairing, as revealed from the DFT calculation (Figure S11). The binding constant between **1d** and **EY** was determined to be 1.2×10^5 M^{-1} (Figure S12). Of note, the distinct red shift of absorption was maintained in the presence of a high concentration of NaCl and bovine serum albumin (Figure S13a,b), which is likely due to the fact that ion pairing induced the formation of nanoaggregates as revealed from transmission electron microscopy (TEM) and dynamic light scattering (DLS) analysis (Figure S13c,d).

Red Light-Enabled Prodrug Activation in Living Cells. On the distinct bathochromic shift of ion pairs, we assumed that the system can be activated by a long-wavelength red light. Surprisingly, even though "**1d** + **EY**" in DMSO shows weak absorbance at 600 nm (molar extinction coefficient ε = 35.5 $M^{-1}\cdot cm^{-1}$, Figure S14a) and "**1d** + **RB**" in DMSO has low absorption at 630 nm (ε = 41.8 $M^{-1}\cdot cm^{-1}$, Figure S14b), the thiol reactivity of **1d** can be successfully activated by 600 and 630 nm red light irradiation, respectively (Figure S15a,b). Particularly, in the case of **RB** as a photocatalyst at an equal molar concentration to **1d** (100 μM), it showed >95% reaction yield within 3 min of 630 nm light irradiation (Figure S15b). In aqueous solution, red light can activate the thiol reactivity of **1d** as well (Figure S16).

Then we examined whether red light can trigger the release of active gold species in living systems. Since no small molecule probe is available to detect reactive gold species in living cells, an engineered *Escherichia coli* strain carrying the GolS-mCherry system was employed.[74] GolS is a sensory protein specific to gold, and it functions as a transcriptional regulator induced by gold ions, promoting the expression of the downstream red fluorescence protein (mCherry) gene (Figure 4 inset). This enables the highly sensitive and selective detection of active gold species but not the inert ones. The *E. coli* cells were incubated with **1d**, **EY**, or both of them for 30 min in Luria−Bertani medium and then irradiated with 600 nm light for 1 h before another 12 h of incubation. As shown by the results in Figure 4, there was no noticeable red fluorescence from the engineered *E. coli* cells with **1d** in the dark. Instead, strong red fluorescence of living *E. coli* cells was observed in the presence of **1d** and **EY** and under red light irradiation. In the absence of either **1d**, **EY**, or light, negligible fluorescence could be found. Therefore, while the gold(III)-hydride complex is stable in living cells in the dark, it can be converted into active gold species by red light irradiation in the presence of **EY**. In the literature, the thiol-reactive gold is known to inhibit TrxR and cancer cell proliferation.[39,75] Indeed, the TrxR inhibitory activity and cytotoxicity of **1d** was activated by **EY** under 600 nm light irradiation (Figure S17a, b).

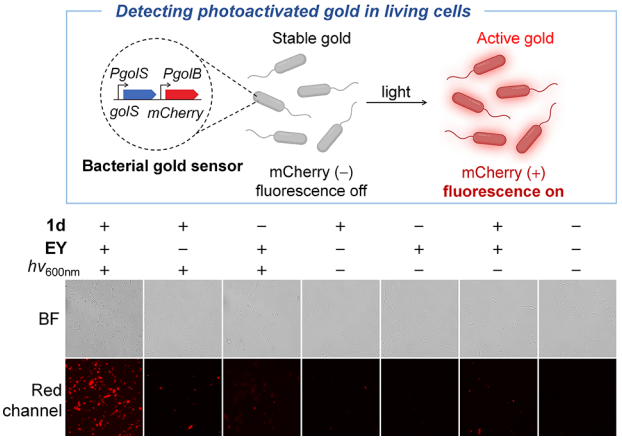

Figure 4. Detecting active gold in living systems. A GolS-mCherry system selectively responds to reactive gold species by expressing red-fluorescent mCherry (inset). The *E. coli* cells the containing GolS-mCherry system showed selective turn-on of red emission in the presence of **1d** (100 μM) and **EY** (100 μM) and under 600 nm red light irradiation. In the absence of either **1d**, **EY**, or light, red fluorescence cannot generate the red fluorescence.

Targeted Activation under an Acidic Tumor Microenvironment. As mentioned before, the ion-pairing-associated red shift of absorption is based on the cationic morpholinium moiety in **1d** with anionic **EY**, where morpholine has a pK_a of 6.9. Based on the chemical equilibrium for morpholine hydrolysis (Figure 5a), the fraction of the hydrolyzed cationic form (δ_{MorH^+}) only accounts for 0.24 of the total morpholine at physiological pH 7.4 (total amount is 1), that is, a major amount (0.76) of **1d** is in the charge-neutral state and cannot form ionic interactions with **EY**. The plot of the distribution coefficient of δ_{MorH^+} versus pH gives a steep change of the $MorH^+$ fraction under the slightly acidic condition. For example, at pH 6.5, the $MorH^+$ fraction increases to 0.72, and at pH 5.5, the cationic fraction is further increased to 0.96. Since **EY** is highly acidic with pK_as of 2.0 and 3.8, **EY** should mostly be in the anionic state under weakly acidic conditions. Therefore, the ionic interactions between **1d** and **EY** should be strongly pH-dependent in a weakly acidic environment.

To test this hypothesis, the UV−vis absorption spectra of **1d** and **EY** under different pH values (aqueous solution containing NaCl) were recorded. As shown in Figures 5b and S18a,b, there are significant increases of absorbance in the bathochromic-shifted region upon lowering the pH. For example, at pH 7.4, the OD_{600nm} is 0.08, which increased to 0.26 and 0.30 at pH values of 6.5 and 5.5, respectively. At pH 5.1, a maximal OD_{600nm} was obtained, while further decreasing the pH did not favor ionic pairing probably because **EY** cannot maintain the anionic state in strong acidic conditions (Figure S18a,b).

It is known that elevated acidity was found in various disease tissues including those of cancer, inflammation, arthritis, and

https://doi.org/10.1021/jacs.4c00408
J. Am. Chem. Soc. 2024, 146, 8547−8556

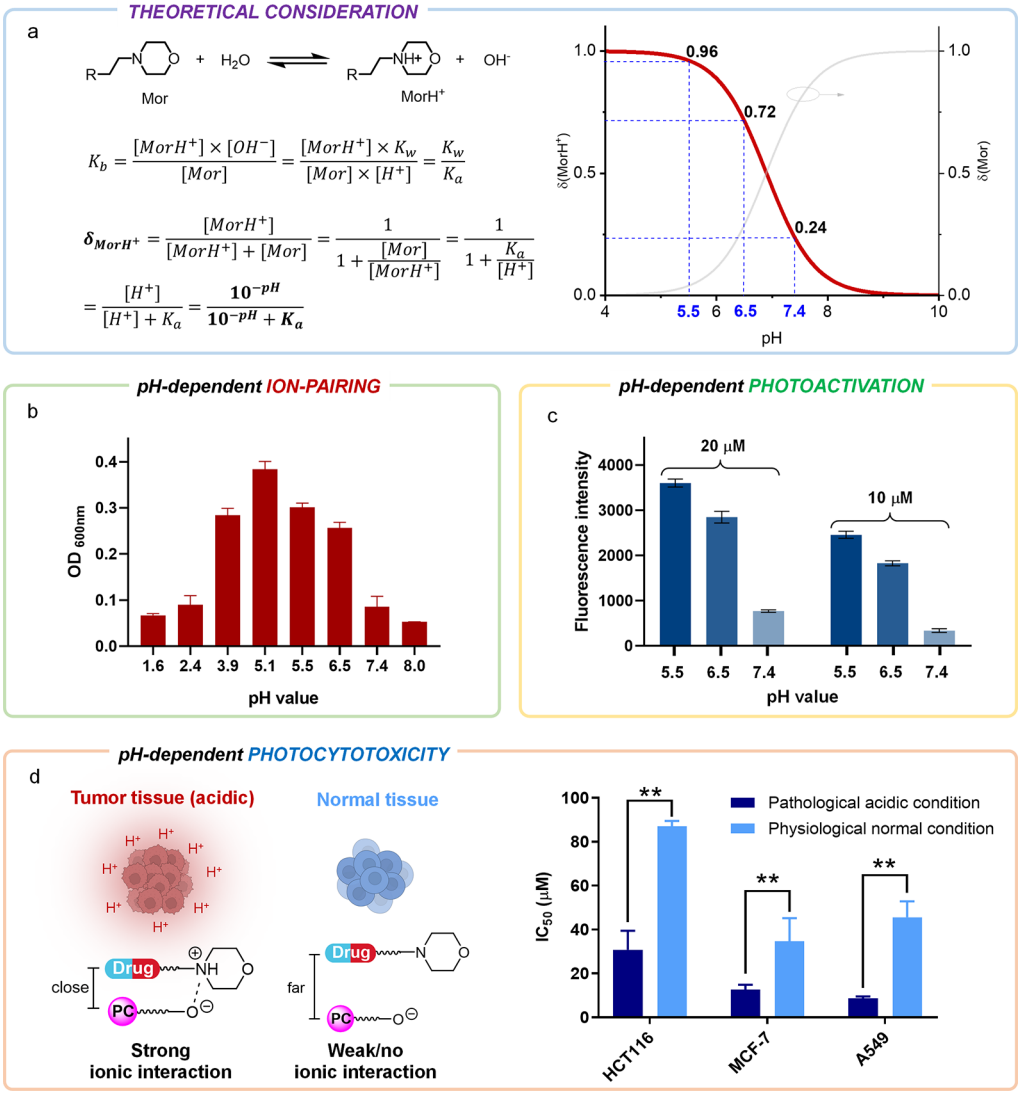

Figure 5. Tumor-targeted photocatalytic prodrug activation. (a) Theoretical calculation for the equilibrium of morpholine (Mor) hydrolysis in aqueous solution, showing a high increase of the cationic $MorH^+$ content under slightly acidic conditions. (b) Absorbance of the **1d** and **EY** in aqueous solution (with 0.1 M NaCl) at the red color region. (c) Emission intensity of GolS-mCherry *E. coli* cells treated with "**1d** + **EY**"-600 nm light at different pH. (d) Inhibition of cell growth after treating cancer cells at different pH.

ischemia.[76] In tumor tissues, the local microenvironment has an acidic pH ranging from 5.5 to 7.0.[77] In this regard, we chose pH values of 5.5 and 6.5 as compared to 7.4 to examine the activation efficiency in living cells. To our delight, the GolS-mCherry *E. coli* cells displayed an obvious pH-dependent red fluorescence (Figure 5c), with intensity increased by 3.4-fold and 4.5-fold at pH 6.5 and 5.5 relative to that at pH 7.4, respectively, at 20 μM of **1d** (similarly at 10 μM), which is in good agreement with the strength of ion pairing as calculated (Figure 5a) and measured (Figure 5b).

Then we examined whether the antitumor effect under an acidic environment had a better performance than the physiological pH. We exploited the red light-activated cytotoxicity of "**1d** + **EY**" against colon carcinoma HCT116, breast cancer MCF-7, and human non-small-cell lung cancer A549 cell lines by MTT assays with a pH at 5.5 as an example. As shown in Figure 5d and Table S1, the cell viability was increased by 3-, 2.5-, and 4.5-fold at acidic pH compared to the neutral conditions for HCT116, MCF-7, and A549 cells, respectively. Similar increments of photocytotoxicity were found at pH 6.5 (Figure S19). Thus, the ion-pairing effects based on a pH-sensitive morpholine-containing prodrug and **EY** may indeed render a targeted prodrug activation by red light in an acidic tumor microenvironment.

Afterward, we tested whether **1d** can be selectively activated by red light in vivo. A zebrafish-based tumor xenograft model, which can mimic the tumor microenvironment, was established.[78,79] HCT116 cells stably expressing EGFP (by the CMV promoter) were injected into the yolk sac of new-born wild-type zebrafish with immature immune systems. 1 day later, the tumor-bearing zebrafish was treated with "**1d** + **RB**" (**RB** was used to avoid the green emission interference of **EY**), which was followed by 630 nm light irradiation for 30 min. As shown by the results in Figure 6a,c(i), the green emission almost fully vanished in the "**1d** + **RB**"-630 nm group compared to the groups in the absence of either **1d**, **RB**, or light irradiation, suggesting the effective release of active gold in the tumor model. Since previous reports have demonstrated that active gold can effectively inhibit blood vessel formation that is associated with tumor angiogenesis in zebrafish,[39,80−82]

https://doi.org/10.1021/jacs.4c00408
J. Am. Chem. Soc. 2024, 146, 8547−8556

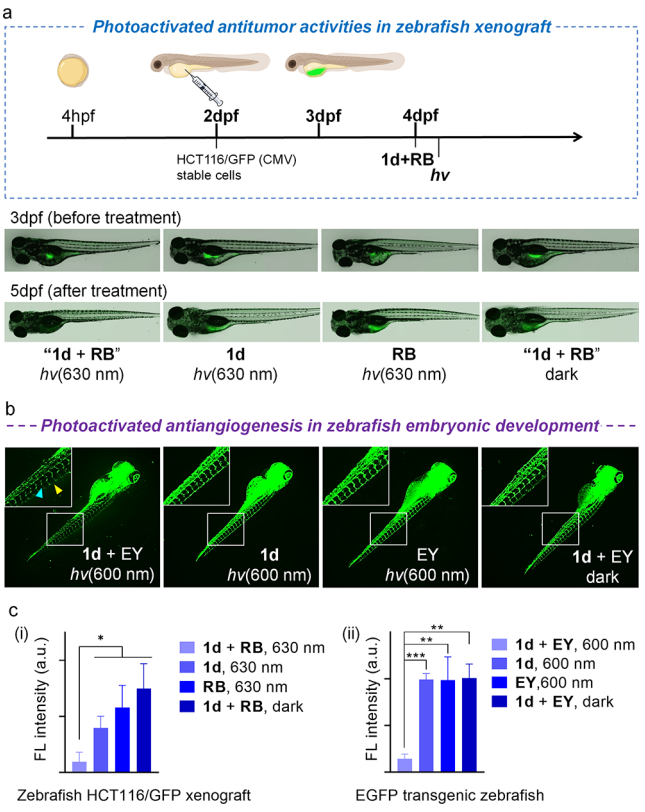

Figure 6. Antitumor activities in zebrafish models. (a) Inhibition of tumor growth by 630 nm light-activated "**1d** (40 μM) + **RB** (40 μM)" in zebrafish bearing HCT116/GFP xenografts. (b) Antiangiogenic activity by 600 nm light-activated "**1d** (100 μM) + **EY** (100 μM)" in Tg (flk1-EGFP)^{S843} transgenic zebrafish. The yellow and blue arrows refer to dorsal longitudinal anastomotic vessel (DLAV) and intersegmental vessel (ISV), respectively. (c) Quantified fluorescence intensity (averaged) in zebrafish HCT116/GFP xenograft (i) and transgenic zebrafish (ii) models.

we further studied the activity of "**1d** + **EY**" on blood vessel formation during zebrafish development. The Tg (flk1-EGFP)^{S843} transgenic zebrafish embryos were treated with "**1d** + **EY**" or the same concentration of single **1d**, **EY**, or solvent for 1 h, followed by 600 nm light irradiation for 30 min. After a total of 5 days of embryo development, the fluorescence images were collected. As exhibited in Figure 6b,c(ii), the vasculature system in "**1d** + **EY**"-treated zebrafish plus red-light irradiation was significantly impaired, especially in the DLAV and ISV. For comparison, the blood vessels of zebrafish in the group treated with **1d** alone, **EY** alone, or without light were growing normally, indicating the effective release of active gold species in zebrafish.

Ion-Pairing Phenomena between EY and Clinic Drugs, Photocages, and Precursors of Labeling Agents. As mentioned before, the pH-dependent bathochromic shift is induced by the morpholine moiety, which is a well-known functional group in a number of clinical and experimental drugs for treatment of cancer, infectious diseases, central nervous system disease, etc.[83] We tested if those morpholine-containing drugs display a similar pH-dependent absorption change by using alectinib and gefitinib, two clinic drugs for non-small-cell lung cancer as examples. As shown in Figure S20a–d, both compounds showed a significant red shift of absorption, which is concentration- and pH-dependent. Interestingly, similar bathochromic shifts were found in the secondary-amine-containing mitoxantrone (Figure 7a). In addition to therapeutic drugs, the morpholine-containing

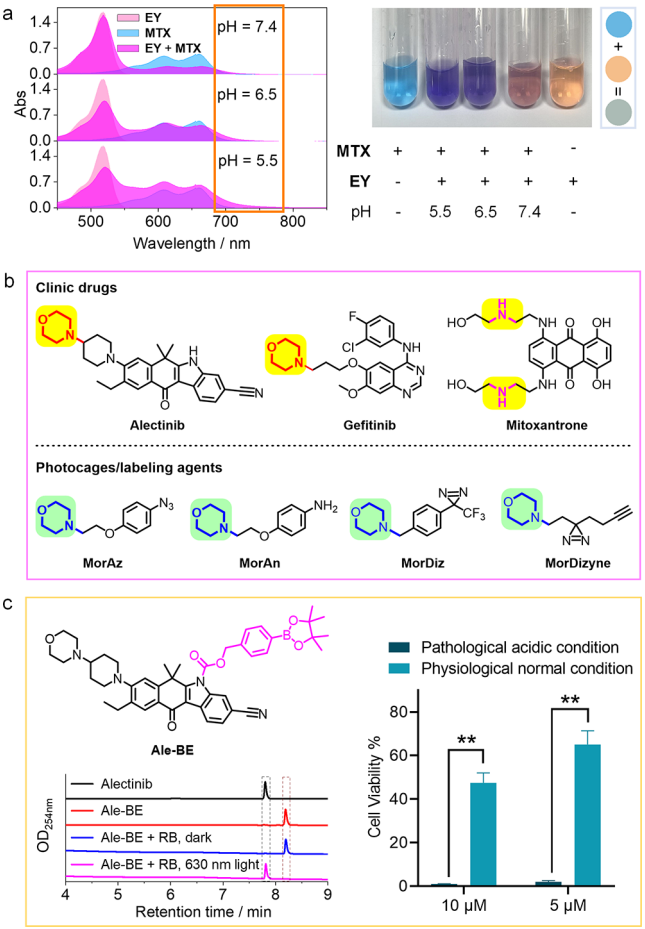

Figure 7. Ion-pairing interactions with other biorelevant molecules. (a) UV–vis absorption spectra for the mixture of **EY** and mitoxantrone (MTX) at different pH. The images for the solution are also shown. (b) Chemical structures of the morpholine (amine)-containing clinic drugs, caged groups, and precursors of reactive labeling agents, all showing acid-driven ion-pairing phenomena. (c) Chemical structure of **Ale-BE**, its photochemical conversion into alectinib by **RB** under 630 nm irradiation for 30 min, and the relative viability of H3122 cells treated with "**Ale-BE** + **RB**" and under 630 nm irradiation for 60 min.

phenyl azide, aniline, trifluoromethylphenyldiazirine, and diazirin-alkyne (Figure 7B), which can act as caged groups and/or photolabeling agents,[84] also formed ion pairs selectively at weak acidic pH (Figure S21a–d). In particular, a boronic ester-caged alectinib prodrug (**Ale-BE**) was synthesized (Figure 7c), which similarly displayed an acid-favored red shift of absorbance with **EY** and **RB** (Figure S20e,f) and can be efficiently converted into alectinib by, for example, **RB** under 630 nm irradiation. A selective cytotoxicity to lung cancer H3122 cells (EML4-ALK rearranged) was found under acidic conditions (Figure 7c and Table S2). Also, a pH-dependent photoreactivity of **MorAn** and **MorDiz** to oligonucleotides was found (Figure S22). These preliminary results suggest that the ion-pair strategy may have applications in targeted activation of different prodrugs and in localized proteome mapping.[78]

https://doi.org/10.1021/jacs.4c00408
J. Am. Chem. Soc. 2024, 146, 8547–8556

CONCLUSIONS

In summary, we have uncovered a feasible strategy for targeted activation of morpholine-containing prodrugs by red light with high efficiency. This was achieved by introducing the photosensitizer **EY/RB** that could form ion pairs with the morpholine-containing gold(III)-hydride prodrug **1d** and efficiently activate the thiol reactivity and anticancer activity of this gold prodrug. Of note, the morpholine moiety renders the ion-pairing effect to be pH-sensitive, and a significant bathochromic shift of absorption tailing to the deep-red region was found under slightly acidic conditions. This results in selective formation of ion pairs in the tumor acidic microenvironment rather than weakly alkaline normal sites, showing prominent and targeted phototherapeutic efficacy to cancer cells in vitro and in vivo. In view that the ion-pairing phenomena were similarly found in morpholine (amine)-containing clinic drugs, photocages, and precursors of reactive labeling agents, it is believed that this ion-pair strategy may afford ample opportunities not only for targeted drug activation but also in mapping of interactomes within localized surroundings.

ASSOCIATED CONTENT

Supporting Information

The Supporting Information is available free of charge at https://pubs.acs.org/doi/10.1021/jacs.4c00408.

Materials and methods, experimental procedures for the gold complex synthesis, characterization, photoreactions, cell-based biological experiments, zebrafish experiments, and supporting figures and tables (PDF)

AUTHOR INFORMATION

Corresponding Authors

Wei Wei − *State Key Laboratory of Coordination Chemistry, School of Life Sciences, Nanjing University, Nanjing 210023, China;* orcid.org/0000-0003-0845-0527; Email: weiwei@nju.edu.cn

Taotao Zou − *Guangdong Provincial Key Laboratory of Chiral Molecule and Drug Discovery, State Key Laboratory of Anti-Infective Drug Discovery and Development, School of Pharmaceutical Sciences, Sun Yat-Sen University, Guangzhou 510006, China; Guangdong Provincial Key Laboratory of Functional Supramolecular Coordination Materials and Applications, Jinan University, Guangzhou 510632, China;* orcid.org/0000-0001-9129-4398; Email: zoutt3@mail.sysu.edu.cn

Authors

Zhiying Xie − *Guangdong Provincial Key Laboratory of Chiral Molecule and Drug Discovery, State Key Laboratory of Anti-Infective Drug Discovery and Development, School of Pharmaceutical Sciences, Sun Yat-Sen University, Guangzhou 510006, China*

Bei Cao − *Warshel Institute for Computational Biology, and General Education Division, The Chinese University of Hong Kong, Shenzhen 518172, China; School of Education Sciences, The Hong Kong University of Science and Technology (Guangzhou), Guangzhou 511453, China*

Jing Zhao − *State Key Laboratory of Coordination Chemistry, School of Life Sciences, Nanjing University, Nanjing 210023, China*

Moyi Liu − *Guangdong Provincial Key Laboratory of Chiral Molecule and Drug Discovery, State Key Laboratory of Anti-Infective Drug Discovery and Development, School of Pharmaceutical Sciences, Sun Yat-Sen University, Guangzhou 510006, China*

Yuhan Lao − *Guangdong Provincial Key Laboratory of Chiral Molecule and Drug Discovery, State Key Laboratory of Anti-Infective Drug Discovery and Development, School of Pharmaceutical Sciences, Sun Yat-Sen University, Guangzhou 510006, China*

Hejiang Luo − *Guangdong Provincial Key Laboratory of Chiral Molecule and Drug Discovery, State Key Laboratory of Anti-Infective Drug Discovery and Development, School of Pharmaceutical Sciences, Sun Yat-Sen University, Guangzhou 510006, China;* Present Address: Faculty of Life Science and Technology, Kunming University of Science and Technology, Kunming, 650500, P.R. China; orcid.org/0009-0003-1465-2704

Zhi Zhong − *Guangdong Provincial Key Laboratory of Chiral Molecule and Drug Discovery, State Key Laboratory of Anti-Infective Drug Discovery and Development, School of Pharmaceutical Sciences, Sun Yat-Sen University, Guangzhou 510006, China*

Xiaolin Xiong − *Guangdong Provincial Key Laboratory of Chiral Molecule and Drug Discovery, State Key Laboratory of Anti-Infective Drug Discovery and Development, School of Pharmaceutical Sciences, Sun Yat-Sen University, Guangzhou 510006, China*

Complete contact information is available at: https://pubs.acs.org/10.1021/jacs.4c00408

Author Contributions

[¶]Z.X., B.C., J.Z., and M.L. contributed equally.

Notes

The authors declare no competing financial interest.

ACKNOWLEDGMENTS

This work is financially supported by the National Natural Science Foundation of China (nos. 22122706 and 22377154), Major Program of Guangzhou National Laboratory (GZNL2023A02012), Guangdong Science and Technology Department (no. 2019QN01C125), Guangdong Basic and Applied Basic Research Foundation (no. 2021A1515012347), Guangzhou Science and Technology Projects (no. 2024A04J6478), Guangdong Provincial Key Laboratory of Construction Foundation (no. 2023B1212060022), and the Open Fund of Guangdong Provincial Key Laboratory of Functional Supramolecular Coordination Materials and Applications (no. 2020B121201005). The Warshel Institute for Computational Biology funding from Shenzhen City and Longgang District is also acknowledged.

REFERENCES

(1) Chen, Y.; Kamlet, A. S.; Steinman, J. B.; Liu, D. R. A biomolecule-compatible visible-light-induced azide reduction from a DNA-encoded reaction-discovery system. *Nat. Chem.* **2011**, *3*, 146−153.

(2) Wang, X.; Wang, X.; Jin, S.; Muhammad, N.; Guo, Z. Stimuli-Responsive Therapeutic Metallodrugs. *Chem. Rev.* **2019**, *119*, 1138−1192.

(3) Shi, H.; Sadler, P. J. How promising is phototherapy for cancer? *Br. J. Cancer* **2020**, *123*, 871−873.

(4) Tay, N. E. S.; Ryu, K. A.; Weber, J. L.; Olow, A. K.; Cabanero, D. C.; Reichman, D. R.; Oslund, R. C.; Fadeyi, O. O.; Rovis, T. Targeted activation in localized protein environments via deep red photoredox catalysis. *Nat. Chem.* **2023**, *15*, 101−109.
(5) Knoll, J. D.; Albani, B. A.; Turro, C. New Ru(II) Complexes for Dual Photoreactivity: Ligand Exchange and $^1O_2$ Generation. *Acc. Chem. Res.* **2015**, *48*, 2280−2287.
(6) Huang, H.; Banerjee, S.; Qiu, K.; Zhang, P.; Blacque, O.; Malcomson, T.; Paterson, M. J.; Clarkson, G. J.; Staniforth, M.; Stavros, V. G.; Gasser, G.; Chao, H.; Sadler, P. J. Targeted photoredox catalysis in cancer cells. *Nat. Chem.* **2019**, *11*, 1041−1048.
(7) Imberti, C.; Zhang, P.; Huang, H.; Sadler, P. J. New Designs for Phototherapeutic Transition Metal Complexes. *Angew. Chem., Int. Ed.* **2020**, *59*, 61−73.
(8) Deng, Z.; Li, H.; Chen, S.; Wang, N.; Liu, G.; Liu, D.; Ou, W.; Xu, F.; Wang, X.; Lei, D.; Lo, P.-C.; Li, Y. Y.; Lu, J.; Yang, M.; He, M.-L.; Zhu, G. Near-infrared-activated anticancer platinum(IV) complexes directly photooxidize biomolecules in an oxygen-independent manner. *Nat. Chem.* **2023**, *15*, 930−939.
(9) Bonnet, S. Ruthenium-Based Photoactivated Chemotherapy. *J. Am. Chem. Soc.* **2023**, *145*, 23397−23415.
(10) Zhang, R.; Xu, H.; Yao, Y.; Ran, G.; Zhang, W.; Zhang, J.; Sessler, J. L.; Gao, S.; Zhang, J.-L. Nickel(II) Phototheranostics: A Case Study in Photoactivated H_2O_2-Enhanced Immunotherapy. *J. Am. Chem. Soc.* **2023**, *145*, 23257−23274.
(11) Shi, G.; Monro, S.; Hennigar, R.; Colpitts, J.; Fong, J.; Kasimova, K.; Yin, H.; DeCoste, R.; Spencer, C.; Chamberlain, L.; Mandel, A.; Lilge, L.; McFarland, S. A. Ru(II) dyads derived from α-oligothiophenes: A new class of potent and versatile photosensitizers for PDT. *Coord. Chem. Rev.* **2015**, *282*−*283*, 127−138.
(12) Wu, Y.; Li, S.; Chen, Y.; He, W.; Guo, Z. Recent advances in noble metal complex based photodynamic therapy. *Chem. Sci.* **2022**, *13*, 5085−5106.
(13) Xue, X.; Qian, C.; Fang, H.; Liu, H.-K.; Yuan, H.; Guo, Z.; Bai, Y.; He, W. Photoactivated Lysosomal Escape of a Monofunctional Pt^{II} Complex Pt-BDPA for Nucleus Access. *Angew. Chem., Int. Ed.* **2019**, *58*, 12661−12666.
(14) Li, M.; Xu, Y.; Pu, Z.; Xiong, T.; Huang, H.; Long, S.; Son, S.; Yu, L.; Singh, N.; Tong, Y.; Sessler, J. L.; Peng, X.; Kim, J. S. Photoredox catalysis may be a general mechanism in photodynamic therapy. *Proc. Natl. Acad. Sci. U.S.A.* **2022**, *119*, No. e2210504119.
(15) Zhou, X.-Q.; Wang, P.; Ramu, V.; Zhang, L.; Jiang, S.; Li, X.; Abyar, S.; Papadopoulou, P.; Shao, Y.; Bretin, L.; Siegler, M. A.; Buda, F.; Kros, A.; Fan, J.; Peng, X.; Sun, W.; Bonnet, S. In vivo metallophilic self-assembly of a light-activated anticancer drug. *Nat. Chem.* **2023**, *15*, 980−987.
(16) van Rixel, V. H. S.; Ramu, V.; Auyeung, A. B.; Beztsinna, N.; Leger, D. Y.; Lameijer, L. N.; Hilt, S. T.; Le Dévédec, S. E.; Yildiz, T.; Betancourt, T.; Gildner, M. B.; Hudnall, T. W.; Sol, V.; Liagre, B.; Kornienko, A.; Bonnet, S. Photo-Uncaging of a Microtubule-Targeted Rigidin Analogue in Hypoxic Cancer Cells and in a Xenograft Mouse Model. *J. Am. Chem. Soc.* **2019**, *141*, 18444−18454.
(17) Toupin, N.; Steinke, S. J.; Nadella, S.; Li, A.; Rohrabaugh, T. N.; Samuels, E. R.; Turro, C.; Sevrioukova, I. F.; Kodanko, J. J. Photosensitive Ru(II) Complexes as Inhibitors of the Major Human Drug Metabolizing Enzyme CYP3A4. *J. Am. Chem. Soc.* **2021**, *143*, 9191−9205.
(18) Steinke, S. J.; Piechota, E. J.; Loftus, L. M.; Turro, C. Acetonitrile Ligand Photosubstitution in Ru(II) Complexes Directly from the ^{3}MLCT State. *J. Am. Chem. Soc.* **2022**, *144*, 20177−20182.
(19) Amarsy, I.; Papot, S.; Gasser, G. Stimuli-Responsive Metal Complexes for Biomedical Applications. *Angew. Chem., Int. Ed.* **2022**, *61*, No. e202205900.
(20) Farrer, N. J.; Woods, J. A.; Salassa, L.; Zhao, Y.; Robinson, K. S.; Clarkson, G.; Mackay, F. S.; Sadler, P. J. A Potent Trans-Diimine Platinum Anticancer Complex Photoactivated by Visible Light. *Angew. Chem., Int. Ed.* **2010**, *49*, 8905−8908.
(21) Barragan, F.; Lopez-Senin, P.; Salassa, L.; Betanzos-Lara, S.; Habtemariam, A.; Moreno, V.; Sadler, P. J.; Marchan, V. Photo-controlled DNA binding of a receptor-targeted organometallic ruthenium(II) complex. *J. Am. Chem. Soc.* **2011**, *133*, 14098−14108.
(22) Albani, B. A.; Peña, B.; Leed, N. A.; de Paula, N. A. B. G.; Pavani, C.; Baptista, M. S.; Dunbar, K. R.; Turro, C. Marked Improvement in Photoinduced Cell Death by a New Tris-heteroleptic Complex with Dual Action: Singlet Oxygen Sensitization and Ligand Dissociation. *J. Am. Chem. Soc.* **2014**, *136*, 17095−17101.
(23) Arora, K.; Herroon, M.; Al-Afyouni, M. H.; Toupin, N. P.; Rohrabaugh, T. N.; Loftus, L. M.; Podgorski, I.; Turro, C.; Kodanko, J. J. Catch and Release Photosensitizers: Combining Dual-Action Ruthenium Complexes with Protease Inactivation for Targeting Invasive Cancers. *J. Am. Chem. Soc.* **2018**, *140*, 14367−14380.
(24) Norman, D. J.; Gambardella, A.; Mount, A. R.; Murray, A. F.; Bradley, M. A Dual Killing Strategy: Photocatalytic Generation of Singlet Oxygen with Concomitant Pt^{IV} Prodrug Activation. *Angew. Chem., Int. Ed.* **2019**, *58*, 14189−14192.
(25) Zhang, L.; Wang, P.; Zhou, X.-Q.; Bretin, L.; Zeng, X.; Husiev, Y.; Polanco, E. A.; Zhao, G.; Wijaya, L. S.; Biver, T.; Le Dévédec, S. E.; Sun, W.; Bonnet, S. Cyclic Ruthenium-Peptide Conjugates as Integrin-Targeting Phototherapeutic Prodrugs for the Treatment of Brain Tumors. *J. Am. Chem. Soc.* **2023**, *145*, 14963−14980.
(26) Askes, S. H. C.; Reddy, G. U.; Wyrwa, R.; Bonnet, S.; Schiller, A. Red Light-Triggered CO Release from $Mn_2(CO)_{10}$ Using Triplet Sensitization in Polymer Nonwoven Fabrics. *J. Am. Chem. Soc.* **2017**, *139*, 15292−15295.
(27) Wang, Z.; Wang, N.; Cheng, S.-C.; Xu, K.; Deng, Z.; Chen, S.; Xu, Z.; Xie, K.; Tse, M.-K.; Shi, P.; Hirao, H.; Ko, C.-C.; Zhu, G. Phorbiplatin, a Highly Potent Pt(IV) Antitumor Prodrug That Can Be Controllably Activated by Red Light. *Chem* **2019**, *5*, 3151−3165.
(28) Deng, Z.; Wang, N.; Liu, Y.; Xu, Z.; Wang, Z.; Lau, T.-C.; Zhu, G. A Photocaged, Water-Oxidizing, and Nucleolus-Targeted Pt(IV) Complex with a Distinct Anticancer Mechanism. *J. Am. Chem. Soc.* **2020**, *142*, 7803−7812.
(29) Hakkennes, M. L. A.; Meijer, M. S.; Menzel, J. P.; Goetz, A.-C.; Van Duijn, R.; Siegler, M. A.; Buda, F.; Bonnet, S. Ligand Rigidity Steers the Selectivity and Efficiency of the Photosubstitution Reaction of Strained Ruthenium Polypyridyl Complexes. *J. Am. Chem. Soc.* **2023**, *145*, 13420−13434.
(30) Alonso-de Castro, S.; Ruggiero, E.; Ruiz-de-Angulo, A.; Rezabal, E.; Mareque-Rivas, J. C.; Lopez, X.; López-Gallego, F.; Salassa, L. Riboflavin as a bioorthogonal photocatalyst for the activation of a Pt^{IV} prodrug. *Chem. Sci.* **2017**, *8*, 4619−4625.
(31) Alonso-de Castro, S.; Cortajarena, A. L.; López-Gallego, F.; Salassa, L. Bioorthogonal Catalytic Activation of Platinum and Ruthenium Anticancer Complexes by FAD and Flavoproteins. *Angew. Chem., Int. Ed.* **2018**, *57*, 3143−3147.
(32) Liu, M.; Luo, Y.; Yan, J.; Xiong, X.; Xing, X.; Kim, J. S.; Zou, T. Photoactivation of Boronic Acid Prodrugs via a Phenyl Radical Mechanism: Iridium(III) Anticancer Complex as an Example. *J. Am. Chem. Soc.* **2023**, *145*, 10082−10091.
(33) Luo, Y.; Cao, B.; Zhong, M.; Liu, M.; Xiong, X.; Zou, T. Organogold(III) Complexes Display Conditional Photoactivities: Evolving From Photodynamic into Photoactivated Chemotherapy in Response to O_2 Consumption for Robust Cancer Therapy. *Angew. Chem., Int. Ed.* **2022**, *61*, No. e202212689.
(34) Zhou, H.-X.; Pang, X. Electrostatic Interactions in Protein Structure, Folding, Binding, and Condensation. *Chem. Rev.* **2018**, *118*, 1691−1741.
(35) Earley, J. D.; Zieleniewska, A.; Ripberger, H. H.; Shin, N. Y.; Lazorski, M. S.; Mast, Z. J.; Sayre, H. J.; McCusker, J. K.; Scholes, G. D.; Knowles, R. R.; Reid, O. G.; Rumbles, G. Ion-pair reorganization regulates reactivity in photoredox catalysts. *Nat. Chem.* **2022**, *14*, 746−753.
(36) Takizawa, S.-y.; Okuyama, T.; Yamazaki, S.; Sato, K.-i.; Masai, H.; Iwai, T.; Murata, S.; Terao, J. Ion Pairing of Cationic and Anionic Ir(III) Photosensitizers for Photocatalytic CO_2 Reduction at Lipid-Membrane Surfaces. *J. Am. Chem. Soc.* **2023**, *145*, 15049−15053.

https://doi.org/10.1021/jacs.4c00408
J. Am. Chem. Soc. 2024, 146, 8547−8556

(37) Morack, T.; Mück-Lichtenfeld, C.; Gilmour, R. Bioinspired Radical Stetter Reaction: Radical Umpolung Enabled by Ion-Pair Photocatalysis. *Angew. Chem., Int. Ed.* **2019**, *58*, 1208−1212.
(38) Hickey, J. L.; Ruhayel, R. A.; Barnard, P. J.; Baker, M. V.; Berners-Price, S. J.; Filipovska, A. Mitochondria-targeted chemotherapeutics: the rational design of gold(I) N-heterocyclic carbene complexes that are selectively toxic to cancer cells and target protein selenols in preference to thiols. *J. Am. Chem. Soc.* **2008**, *130*, 12570−12571.
(39) Meyer, A.; Bagowski, C. P.; Kokoschka, M.; Stefanopoulou, M.; Alborzinia, H.; Can, S.; Vlecken, D. H.; Sheldrick, W. S.; Wölfl, S.; Ott, I. On the Biological Properties of Alkynyl Phosphine Gold(I) Complexes. *Angew. Chem., Int. Ed.* **2012**, *51*, 8895−8899.
(40) Zou, T.; Lum, C. T.; Lok, C.-N.; Zhang, J.-J.; Che, C.-M. Chemical biology of anticancer gold(III) and gold(I) complexes. *Chem. Soc. Rev.* **2015**, *44*, 8786−8801.
(41) Lu, Y.; Ma, X.; Chang, X.; Liang, Z.; Lv, L.; Shan, M.; Lu, Q.; Wen, Z.; Gust, R.; Liu, W. Recent development of gold(I) and gold(III) complexes as therapeutic agents for cancer diseases. *Chem. Soc. Rev.* **2022**, *51*, 5518−5556.
(42) Marciano, Y.; del Solar, V.; Nayeem, N.; Dave, D.; Son, J.; Contel, M.; Ulijn, R. V. Encapsulation of Gold-Based Anticancer Agents in Protease-Degradable Peptide Nanofilaments Enhances Their Potency. *J. Am. Chem. Soc.* **2023**, *145*, 234−246.
(43) Berners-Price, S. J.; Mirabelli, C. K.; Johnson, R. K.; Mattern, M. R.; McCabe, F. L.; Faucette, L. F.; Sung, C.-M.; Mong, S.-M.; Sadler, P. J.; Crooke, S. T. In Vivo Antitumor Activity and in Vitro Cytotoxic Properties of Bis[1,2-bis(diphenylphosphino)ethane]gold-(I) Chloride. *Cancer Res.* **1986**, *46*, 5486−5493.
(44) Nobili, S.; Mini, E.; Landini, I.; Gabbiani, C.; Casini, A.; Messori, L. Gold Compounds as Anticancer Agents: Chemistry, Cellular Pharmacology, and Preclinical Studies. *Med. Res. Rev.* **2010**, *30*, 550−580.
(45) Berners-Price, S. J.; Barnard, P. J. Therapeutic Gold Compounds. In *Ligand Design in Medicinal Inorganic Chemistry*; John Wiley & Sons, Ltd, 2014, pp 227−256.
(46) Messori, L.; Scaletti, F.; Massai, L.; Cinellu, M. A.; Russo Krauss, I.; di Martino, G.; Vergara, A.; Paduano, L.; Merlino, A. Interactions of Gold-Based Drugs with Proteins: Crystal Structure of the Adduct Formed Between Ribonuclease A and a Cytotoxic Gold(III) Compound. *Metallomics* **2014**, *6*, 233−236.
(47) Zhang, C.; Fortin, P.-Y.; Barnoin, G.; Qin, X.; Wang, X.; Fernandez Alvarez, A.; Bijani, C.; Maddelein, M.-L.; Hemmert, C.; Cuvillier, O.; Gornitzka, H. An Artemisinin-Derivative-(NHC)Gold-(I) Hybrid with Enhanced Cytotoxicity through Inhibition of NRF2 Transcriptional Activity. *Angew. Chem., Int. Ed.* **2020**, *59*, 12062−12068.
(48) Moreno-Alcántar, G.; Picchetti, P.; Casini, A. Gold Complexes in Anticancer Therapy: From New Design Principles to Particle-Based Delivery Systems. *Angew. Chem., Int. Ed.* **2023**, *62*, No. e202218000.
(49) Mertens, R. T.; Gukathasan, S.; Arojojoye, A. S.; Olelewe, C.; Awuah, S. G. Next Generation Gold Drugs and Probes: Chemistry and Biomedical Applications. *Chem. Rev.* **2023**, *123*, 6612−6667.
(50) Babu, T.; Ghareeb, H.; Basu, U.; Schueffl, H.; Theiner, S.; Heffeter, P.; Koellensperger, G.; Metanis, N.; Gandin, V.; Ott, I.; Schmidt, C.; Gibson, D. Oral Anticancer Heterobimetallic PtIV-AuI Complexes Show High In Vivo Activity and Low Toxicity. *Angew. Chem., Int. Ed.* **2023**, *62*, No. e202217233.
(51) Jiang, J.; Xiong, X.; Zou, T. Modulating the Chemical Reactivity of Gold Complexes in Living Systems: From Concept to Biomedical Applications. *Acc. Chem. Res.* **2023**, *56*, 1043−1056.
(52) López-Hernández, J. E.; Contel, M. Promising heterometallic compounds as anticancer agents: Recent studies in vivo. *Curr. Opin. Chem. Biol.* **2023**, *72*, 102250.
(53) Barnard, P. J.; Wedlock, L. E.; Baker, M. V.; Berners-Price, S. J.; Joyce, D. A.; Skelton, B. W.; Steer, J. H. Luminescence Studies of the Intracellular Distribution of a Dinuclear Gold(I) N-Heterocyclic Carbene Complex. *Angew. Chem., Int. Ed.* **2006**, *45*, 5966−5970.
(54) Ray, S.; Mohan, R.; Singh, J. K.; Samantaray, M. K.; Shaikh, M. M.; Panda, D.; Ghosh, P. Anticancer and Antimicrobial Metallopharmaceutical Agents Based on Palladium, Gold, and Silver N-Heterocyclic Carbene Complexes. *J. Am. Chem. Soc.* **2007**, *129*, 15042−15053.
(55) Marzano, C.; Ronconi, L.; Chiara, F.; Giron, M. C.; Faustinelli, I.; Cristofori, P.; Trevisan, A.; Fregona, D. Gold(III)-dithiocarbamato anticancer agents: activity, toxicology and histopathological studies in rodents. *Int. J. Cancer* **2011**, *129*, 487−496.
(56) Akerman, K. J.; Fagenson, A. M.; Cyril, V.; Taylor, M.; Muller, M. T.; Akerman, M. P.; Munro, O. Q. Gold(III) macrocycles: nucleotide-specific unconventional catalytic inhibitors of human topoisomerase I. *J. Am. Chem. Soc.* **2014**, *136*, 5670−5682.
(57) Fernández-Gallardo, J.; Elie, B. T.; Sadhukha, T.; Prabha, S.; Sanaú, M.; Rotenberg, S. A.; Ramos, J. W.; Contel, M. Heterometallic titanium-gold complexes inhibit renal cancer cells in vitro and in vivo. *Chem. Sci.* **2015**, *6*, 5269−5283.
(58) Wirmer-Bartoschek, J.; Bendel, L. E.; Jonker, H. R. A.; Grün, J. T.; Papi, F.; Bazzicalupi, C.; Messori, L.; Gratteri, P.; Schwalbe, H. Solution NMR Structure of a Ligand/Hybrid-2-G-Quadruplex Complex Reveals Rearrangements that Affect Ligand Binding. *Angew. Chem., Int. Ed.* **2017**, *56*, 7102−7106.
(59) Wragg, D.; de Almeida, A.; Bonsignore, R.; Kühn, F. E.; Leoni, S.; Casini, A. On the Mechanism of Gold/NHC Compounds Binding to DNA G-Quadruplexes: Combined Metadynamics and Biophysical Methods. *Angew. Chem., Int. Ed.* **2018**, *57*, 14524−14528.
(60) Guarra, F.; Terenzi, A.; Pirker, C.; Passannante, R.; Baier, D.; Zangrando, E.; Gómez-Vallejo, V.; Biver, T.; Gabbiani, C.; Berger, W.; Llop, J.; Salassa, L. ^{124}I Radiolabeling of a Au^{III}-NHC Complex for In Vivo Biodistribution Studies. *Angew. Chem., Int. Ed.* **2020**, *59*, 17130−17136.
(61) Sen, S.; Hufnagel, S.; Maier, E. Y.; Aguilar, I.; Selvakumar, J.; DeVore, J. E.; Lynch, V. M.; Arumugam, K.; Cui, Z.; Sessler, J. L.; Arambula, J. F. Rationally Designed Redox-Active Au(I) N-Heterocyclic Carbene: An Immunogenic Cell Death Inducer. *J. Am. Chem. Soc.* **2020**, *142*, 20536−20541.
(62) Tong, K.-C.; Lok, C.-N.; Wan, P.-K.; Hu, D.; Fung, Y. M. E.; Chang, X.-Y.; Huang, S.; Jiang, H.; Che, C.-M. An anticancer gold(III)-activated porphyrin scaffold that covalently modifies protein cysteine thiols. *Proc. Natl. Acad. Sci. U.S.A.* **2020**, *117*, 1321.
(63) Arojojoye, A. S.; Olelewe, C.; Gukathasan, S.; Kim, J. H.; Vekaria, H.; Parkin, S.; Sullivan, P. G.; Awuah, S. G. Serum-Stable Gold(III) Bisphosphine Complex Induces Mild Mitochondrial Uncoupling and In Vivo Antitumor Potency in Triple Negative Breast Cancer. *J. Med. Chem.* **2023**, *66*, 7868−7879.
(64) Luo, H.; Cao, B.; Chan, A. S. C.; Sun, R. W.-Y.; Zou, T. Cyclometalated Gold(III)-Hydride Complexes Exhibit Visible Light-Induced Thiol Reactivity and Act as Potent Photo-Activated Anti-Cancer Agents. *Angew. Chem., Int. Ed.* **2020**, *59*, 11046−11052.
(65) Eppel, D.; Rudolph, M.; Rominger, F.; Hashmi, A. S. K. Mercury-Free Synthesis of Pincer [C∧N∧C]Au^{III} Complexes by an Oxidative Addition/CH Activation Cascade. *ChemSusChem* **2020**, *13*, 1986−1990.
(66) Sahoo, R.; Dutta, S.; Pradhan, M.; Ray, C.; Roy, A.; Pal, T.; Pal, A. Arsenate stabilized Cu2O nanoparticle catalyst for one-electron transfer reversible reaction. *Dalton Trans.* **2014**, *43*, 6677−6683.
(67) Hari, D. P.; König, B. Synthetic applications of eosin Y in photoredox catalysis. *Chem. Commun.* **2014**, *50*, 6688−6699.
(68) Romero, N. A.; Nicewicz, D. A. Organic Photoredox Catalysis. *Chem. Rev.* **2016**, *116*, 10075−10166.
(69) Buzzetti, L.; Crisenza, G. E. M.; Melchiorre, P. Mechanistic Studies in Photocatalysis. *Angew. Chem., Int. Ed.* **2019**, *58*, 3730−3747.
(70) Williams, P. J. H.; Boustead, G. A.; Heard, D. E.; Seakins, P. W.; Rickard, A. R.; Chechik, V. New Approach to the Detection of Short-Lived Radical Intermediates. *J. Am. Chem. Soc.* **2022**, *144*, 15969−15976.

https://doi.org/10.1021/jacs.4c00408
J. Am. Chem. Soc. 2024, 146, 8547−8556

(71) Pintus, A.; Bochmann, M. Radical-initiated alkene hydroauration as a route to gold(iii) alkyls: an experimental and computational study. *RSC Adv.* **2018**, *8*, 2795−2803.
(72) Batistela, V. R.; Pellosi, D. S.; de Souza, F. D.; da Costa, W. F.; de Oliveira Santin, S. M.; de Souza, V. R.; Caetano, W.; de Oliveira, H. P. M.; Scarminio, I. S.; Hioka, N. pKa determinations of xanthene derivates in aqueous solutions by multivariate analysis applied to UV-Vis spectrophotometric data. *Spectrochim. Acta, Part A* **2011**, *79*, 889−897.
(73) Rayer, A. V.; Sumon, K. Z.; Jaffari, L.; Henni, A. Dissociation Constants (pKa) of Tertiary and Cyclic Amines: Structural and Temperature Dependences. *J. Chem. Eng. Data* **2014**, *59*, 3805−3813.
(74) Wei, W.; Zhu, T.; Wang, Y.; Yang, H.; Hao, Z.; Chen, P. R.; Zhao, J. Engineering a gold-specific regulon for cell-based visual detection and recovery of gold. *Chem. Sci.* **2012**, *3*, 1780−1784.
(75) Silva, M. J. S. A.; Gois, P. M. P.; Gasser, G. Unveiling the Potential of Transition Metal Complexes for Medicine: Translational in Situ Activation of Metal-Based Drugs from Bench to in Vivo Applications. *ChemBioChem* **2021**, *22*, 1740−1742.
(76) Deacon, J. C.; Engelman, D. M.; Barrera, F. N. Targeting acidity in diseased tissues: Mechanism and applications of the membrane-inserting peptide, pHLIP. *Arch. Biochem. Biophys.* **2015**, *565*, 40−48.
(77) Vaupel, P.; Kallinowski, F.; Okunieff, P. Blood Flow, Oxygen and Nutrient Supply, and Metabolic Microenvironment of Human Tumors: A Review. *Cancer Res.* **1989**, *49*, 6449−6465.
(78) Liu, Z.; Xie, X.; Huang, Z.; Lin, F.; Liu, S.; Chen, Z.; Qin, S.; Fan, X.; Chen, P. R. Spatially resolved cell tagging and surfaceome labeling via targeted photocatalytic decaging. *Chem* **2022**, *8*, 2179−2191.
(79) Chen, X.; Li, Y.; Yao, T.; Jia, R. Benefits of Zebrafish Xenograft Models in Cancer Research. *Front. Cell Dev. Biol.* **2021**, *9*, 616551.
(80) Jiang, J.; Cao, B.; Chen, Y.; Luo, H.; Xue, J.; Xiong, X.; Zou, T. Alkylgold(III) Complexes Undergo Unprecedented Photo-Induced β-Hydride Elimination and Reduction for Targeted Cancer Therapy. *Angew. Chem., Int. Ed.* **2022**, *61*, No. e202201103.
(81) Zhang, J.-J.; Abu el Maaty, M. A.; Hoffmeister, H.; Schmidt, C.; Muenzner, J. K.; Schobert, R.; Wölfl, S.; Ott, I. A Multitarget Gold(I) Complex Induces Cytotoxicity Related to Aneuploidy in HCT-116 Colorectal Carcinoma Cells. *Angew. Chem., Int. Ed.* **2020**, *59*, 16795−16800.
(82) Long, Y.; Cao, B.; Xiong, X.; Chan, A. S. C.; Sun, R. W.-Y.; Zou, T. Bioorthogonal Activation of Dual Catalytic and Anti-Cancer Activities of Organogold(I) Complexes in Living Systems. *Angew. Chem., Int. Ed.* **2021**, *60*, 4133−4141.
(83) Kourounakis, A. P.; Xanthopoulos, D.; Tzara, A. Morpholine as a privileged structure: A review on the medicinal chemistry and pharmacological activity of morpholine containing bioactive molecules. *Med. Res. Rev.* **2020**, *40*, 709−752.
(84) Seath, C. P.; Trowbridge, A. D.; Muir, T. W.; MacMillan, D. W. C. Reactive intermediates for interactome mapping. *Chem. Soc. Rev.* **2021**, *50*, 2911−2926.

https://doi.org/10.1021/jacs.4c00408
J. Am. Chem. Soc. 2024, 146, 8547−8556